NANO LETTERS

2005
Vol. 5, No. 10
1963−1967

Surface Plasmon Standing Waves in Large-Area Subwavelength Hole Arrays

Eun-Soo Kwak,[†,‡] Joel Henzie,[†,‡] Shih-Hui Chang,[‡,§] Stephen K. Gray,[§] George C. Schatz,[‡] and Teri W. Odom*[,‡]

Department of Chemistry, Northwestern University, 2145 Sheridan Road, Evanston, Illinois 60208, and Chemistry Division and Center for Nanoscale Materials, Argonne National Laboratory, Argonne, Illinois 60439

Received July 13, 2005; Revised Manuscript Received August 15, 2005

ABSTRACT

A flexible and parallel procedure to generate large-area, free-standing films of subwavelength hole arrays has been demonstrated. This method is materials-general, and multilayered films of different materials were constructed. The optical quality of these films was tested using a near-field scanning optical microscope, which revealed the formation of surface plasmon standing wave patterns that were consistent with numerical simulations. Because the properties of the holes and the film materials can be easily tailored, new types of plasmonic and photonic devices can be envisioned and tested.

The observation of enhanced transmission through subwavelength hole arrays has generated considerable interest worldwide.[1,2] These arrays make possible new fundamental studies of surface plasmon (SP) interactions with periodic structures[3−5] and novel technologies, including spectroscopically based chemical and biological sensors and photonic devices.[2,6−9] The most common method to fabricate hole arrays is focused ion beam (FIB) milling,[1] a serial and low throughput approach that can control the diameter and spacing of the holes with reasonable precision. Free-standing suspended films have been fabricated by FIB and reactive ion etching, but the generation of multilayered films is challenging and laborious and has been limited to only a few metals.[10] No techniques have been developed for producing optical quality hole arrays in a parallel fashion, over areas larger than hundreds of square microns, and out of multiple materials. The increased access to and expanded capabilities of these nanostructured films are critical for their use in practical photonic devices and in biological and chemical sensing applications.

We have developed a flexible approach to construct large-area, free-standing films of subwavelength hole arrays and have demonstrated their high optical quality. Our procedure has four key advantages over current methods: (1) Use of masters: Masters are high-quality patterns from which many low-cost copies can be duplicated. We used inexpensive masters patterned with arrays of subwavelength features in photoresist over 1 in.[2] that were generated by phase-shifting photolithography (PSP),[11,12] although the procedure is readily applicable to masters prepared by other methods. (2) Parallelism: Poly(dimethylsiloxane) (PDMS) is cast against a master to form an elastomeric mask, which will be used repeatedly to fabricate arrays of structures in the first step of the process. Our method creates all the holes in the array simultaneously rather than by drilling through a film one hole at a time. (3) Simplicity: The strategy uses widely available lithographic techniques such as photolithography, wet chemical etching, and e-beam deposition. (4) Flexibility: Multilayered films of hole arrays consisting of noble metals and magnetic materials can be fabricated with exquisite control over the thickness of each layer.

Large-area films of subwavelength hole arrays were prepared in several steps (Figure 1A). First, a nearly square array of 250-nm circular posts in positive-tone photoresist was patterned on a Si (100) wafer using PSP and a PDMS mask, followed by the e-beam deposition of a thin layer of Cr. After the photoresist was removed, the Cr film was left perforated with round holes having very smooth edges.[13] This Cr layer has two functions: (1) it serves as a template for the hole patterns in the metallic films, and (2) it serves as a sacrificial layer to create free-standing films. Next, the exposed Si was anisotropically etched to form pyramidal pits beneath the Cr holes. This void beneath the holes is crucial for allowing relatively thick films to be created. E-beam evaporation was then used to deposit a single metal or multiple materials of desired thickness (as thick as 500 nm) onto the patterned Cr film. By etching away the Cr film, the metallic film of hole arrays was detached from the Si substrate (Figure 1B). The free-standing films were then

* Corresponding author. E-mail: todom@northwestern.edu.
† These authors contributed equally to this work.
‡ Northwestern University.
§ Argonne National Laboratory.

10.1021/nl051339s CCC: $30.25
Published on Web 09/02/2005

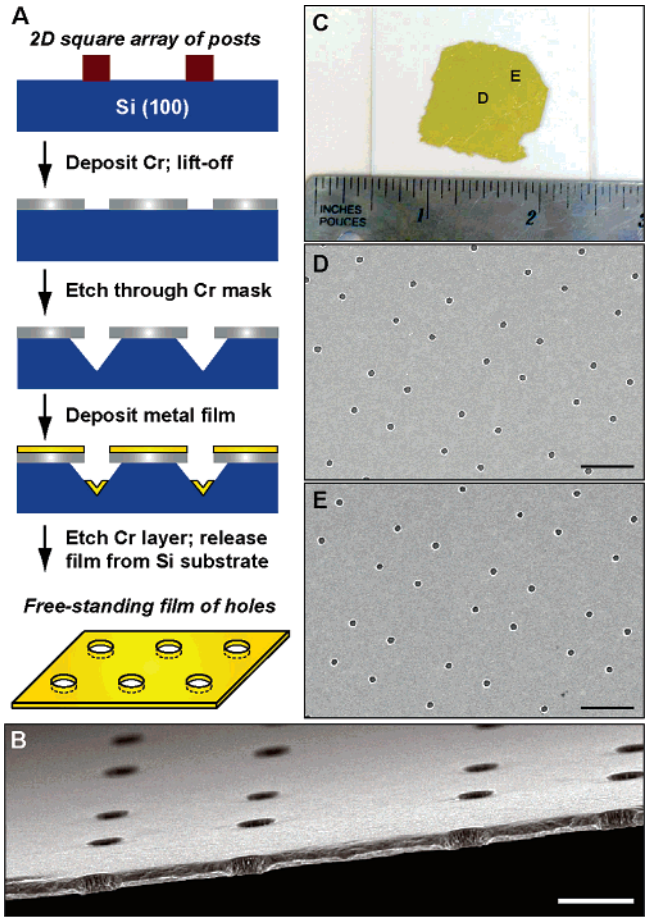

Figure 1. Fabrication and structural characterization of large-area hole arrays. (A) Preparation of free-standing films of subwavelength hole arrays. (B) SEM image of a portion of a free-standing 100-nm Au film perforated with 250-nm holes. Scale bar: 500 nm. (C) Optical micrograph of ~1-in.^{2} free-standing film placed on a glass substrate. (D) and (E) SEM images of representative areas of the film illustrating the uniformity of the patterning. The holes are spaced 1.6 × 2.4 μm. Scale bar: 2 μm.

rinsed several times in Milli-Q water and placed on a glass cover slip to dry. Figure 1C depicts an optical micrograph of a 100-nm thick Au film perforated with 250-nm holes spaced 1.6 × 2.4 μm apart; different, representative areas imaged by scanning electron microscopy (SEM) indicate that this large-area array of holes is nearly defect-free (Figure 1D,E). Unlike most hole arrays fabricated by FIB, the overall topography of these large-area films is flat and very uniform.

To test the optical quality of these films, we investigated their properties using near-field scanning optical microscopy (NSOM). Optically thick Au films having 250-nm holes, sitting on a glass substrate, were analyzed using an NSOM (Aurora III) in illumination mode with Al-coated optical fiber probes. Light (excitation wavelength: λ_{ex}) from a 633-nm HeNe laser or an 800-nm Ti/sapphire laser was coupled into the fiber tip near the air/Au interface, and the transmitted light into the glass substrate was collected in the far-field with an avalanche photodiode. Although far-field light intensity is collected, the optical image, constructed by plotting this light intensity as a function of the probe position, provides information about near-field phenomena. Under

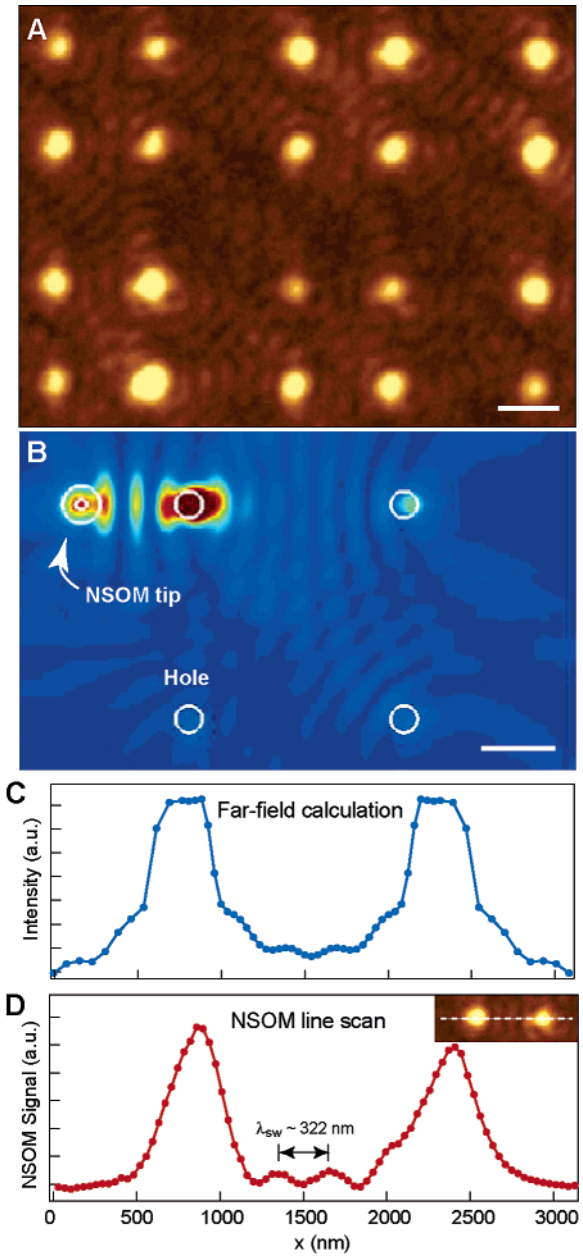

Figure 2. Near-field and far-field optical images and calculations. (A) NSOM optical image of holes in a 100-nm Au film on glass. The image was acquired at a 200 × 200 pixel resolution at a 5-ms/pixel scan rate using an Al-coated probe (tip aperture ≈ 70 nm; Veeco) with an unknown, but fixed, polarization. Scale bar: 1 μm. (B) Calculated near-field SPP standing wave pattern at the Au/air interface for a given NSOM tip position for four 200-nm holes in a 1.6 × 1.6 μm array on a 100-nm Au film supported on glass. Scale bar: 500 nm. (C) Calculated far-field intensity transmitted into the glass substrate of four holes based on separate calculations with the NSOM tip at different positions along the scan line indicated in panel D below. The fringe spacing of $\lambda_{sw} \approx \lambda_{SPP}/2$ is present but is relatively smaller in amplitude compared to the transmission through the holes. (D) Cross-section of two neighboring holes from panel A. The standing waves between the holes have a period of $\lambda_{sw} \approx 322$ nm.

local illumination of 633-nm light, a 100-nm thick Au film (Figure 2A) exhibited enhanced transmission at the holes, which can be attributed to the localized SPs (LSPs) of the holes coupling resonantly with the incident light. Interest-

ingly, fringes reminiscent of standing wave patterns were observed between adjacent holes.

Our results indicate that light from the NSOM tip is locally exciting surface plasmon polariton (SPP) waves on the film surfaces.[14,15] To verify the role of SPPs, we carried out three-dimensional Finite-Difference Time-Domain (FDTD) simulations in a manner similar to those of refs 5 and 15, in which further technical details may be found. The calculations involved a 100-nm Au film with four holes in a square array (1.6-μm center-to-center distance) with air above and a glass substrate below. We also included a model of the NSOM tip, similar to that used in previous calculations[15] but in illumination mode. The incident wave was a fundamental TM_{11} mode of the NSOM fiber core that was launched from the upper part of the tip. SPP waves were generated not only on the top Au/air interface, but also on the bottom Au/glass interface by the NSOM tip because of the finite thickness of the metal film. The SPPs exhibited a $\cos^2\phi$ dependence in intensity along the polarization direction of the incident wave. At each NSOM tip location, the far-field signal was calculated as the surface integral of the Poynting vector in the downward direction, at a distance away from the Au/glass interface. The near-field pattern was plotted as the total electric field intensity on the Au/glass interface.

We found that fringes in the calculated near-field intensity appeared on both the top and the bottom (Figure 2B) metal surfaces because of the interference between the SPP waves generated by the tip and the SPPs reflected by the holes. These standing wave patterns were most pronounced when the NSOM tip was located over a position of the SPP wave that corresponded to the maximum intensity. The fringes produced by the standing wave in the near-field should lead, in the far-field, to intensity maxima with a period (λ_{sw}) that is approximately half of the SPP wavelength ($\lambda_{SPP} = 603$ nm[5]) at the Au film/air interface (Figure 2C); indeed, fringes with $\lambda_{sw} \approx 322$ nm (roughly $\lambda_{SPP}/2$) were measured in the experiment (Figure 2D). The slight difference in the measured period of the fringes and the calculated $\lambda_{SPP}/2$ is not surprising because the fringe pattern follows a Bessel function versus position rather than a $\cos^2$ function.[5] Thus, the first few peaks have a somewhat longer peak-to-peak distance. Note that each point of the theoretical result in Figure 2C represents a separate calculation with the NSOM tip at a different position.

A more quantitative understanding of the NSOM images requires consideration of both the near-field excitation of the hole and the SPP standing waves surrounding the hole. When SPP waves encounter a hole, they are partially reflected back, which leads to standing wave formation, and partially converted into far-field light. LSP resonances at the holes are also excited, and, if the incident light is close to such a LSP resonance ($\lambda_{ex} \approx \lambda_{LSP}$), far-field scattering is enhanced. This scenario describes what we observed in the 100-nm Au film on glass with 250-nm holes (Figure 2A), for which $\lambda_{LSP} \approx 630$ nm, which is close to $\lambda_{ex} = 633$ nm.[5] As the film thickness is decreased, light transmitted directly through the film will, in the far-field, dominate over that coming from SPP scattering at the holes, and the amplitude

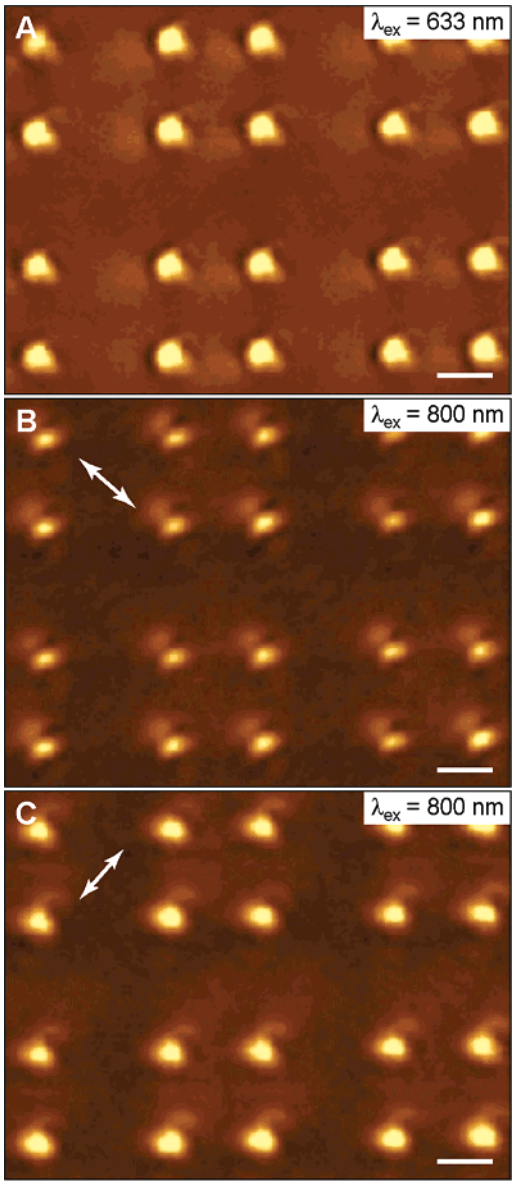

Figure 3. NSOM images of 50-nm Au films with 250-nm holes that were illuminated using (A) $\lambda_{ex} = 633$ and (B,C) $\lambda_{ex} = 800$ nm light. The use of longer wavelength light effectively increases the thickness of the film, so that SPP standing waves can be observed. The white arrows indicate the polarization direction of the tip. (B) Polarization is parallel to the light from the tip. (C) Polarization is perpendicular to the light from the tip. All scale bars: 1 μm.

of the fringe pattern will decrease significantly or disappear—which is what we observed in 50-nm Au films (Figure 3A) using $\lambda_{ex} = 633$ nm. We were able to recover faint fringes in this 50-nm film using $\lambda_{ex} = 800$ nm because less light can penetrate through the Au film at longer wavelengths. Moreover, we selected polarization directions that were relative to the unknown, but fixed, polarization of the tip by placing a polarizer after the film and before the detector. In this way, we observed how the orientation of the fringe patterns changed at different polarizations (Figure 3B,C).

To provide further evidence that the formation of the fringe patterns is a result of interfering SPPs, we prepared and analyzed films of subwavelength hole arrays constructed from layers of different metals, namely, Au and Ni (Figure

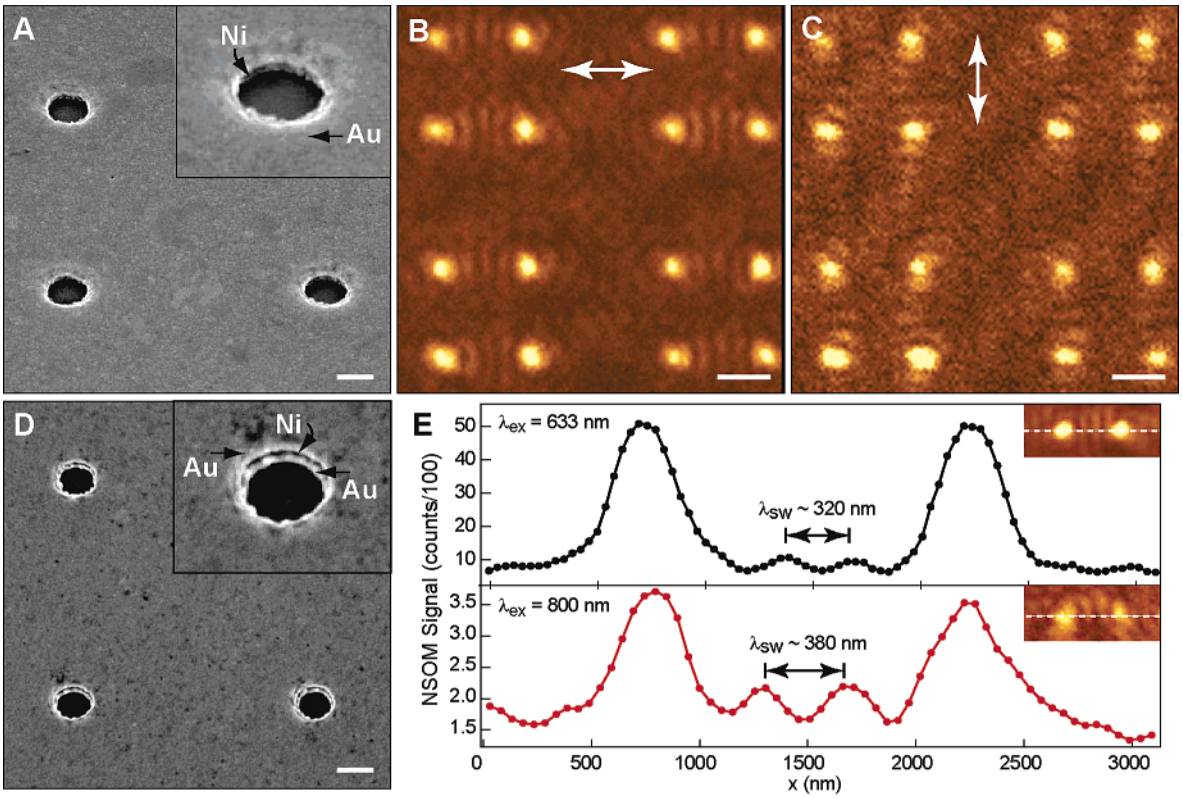

Figure 4. Structural and optical properties of bilayered and multilayered films. (A) SEM image of holes in a Au/Ni (50 nm/50 nm) film. The tilt angle is 35°. Scale bar: 200 nm. (B,C) NSOM images of a Au/Ni film with polarization that is parallel and perpendicular to the light from the tip, respectively. The arrows indicate the direction of polarization; the direction of the fringes rotates along with the changes in polarization. Scale bars: 1 μm. (D) SEM image of 200-nm holes in a Au/Ni/Au (40/20/40) film. The tilt angle is 25°. Scale bar: 200 nm. (E) Cross-section of two neighboring holes in a 40/70/40 film imaged under local $\lambda_{ex} = 633$ and 800 nm light. The period (λ_{sw}) of the SPP standing wave between the holes increases as the excitation wavelength increases.

4A,D). We chose Ni because it exhibits a complex dielectric constant that is different from Au in the wavelengths of our experiments[16] and because it can function as an absorbing layer. A 100-nm thick bilayer film made of 50-nm Au and 50-nm Ni (Au/Ni; 50/50) was tested in the NSOM in two different configurations. In the first case, the film was placed on a glass substrate with the Ni side facing up (the Au side was against the glass). No fringe patterns were observed because no SPPs were excited in the Ni film. In the second case, the bilayer film was placed on the glass with the Au side facing up, and standing wave patterns were observed between the holes. We also investigated their dependence on polarization (Figure 4B,C), and the directional dependence of the patterns clearly supports that the standing waves can be attributed to SPP propagation combined with scattering from the holes.

In addition, we constructed films of hole arrays consisting of three layers to show the versatility of our procedure. These multilayered films (Au/Ni/Au) consisted of a Ni core sandwiched between two layers of Au with thicknesses of 40/20/40 nm (Figure 4D) and 40/70/40 nm. Under $\lambda_{ex} = 633$ nm light, both films exhibited standing wave patterns with a period of $\lambda_{sw} \approx 320$ nm (Figure 4E), which is nearly identical to the pure Au film case. We also imaged the 40/70/40 film with $\lambda_{ex} = 800$ nm ($\lambda_{SPP} \approx 784$ nm[5]) and observed fringes with an increased spacing of $\lambda_{sw} \approx 380$ nm, which is $\sim\lambda_{SPP}/2$ at this excitation wavelength (Figure 4E) and consistent with our theoretical model.

This letter has shown a materials-general procedure to prepare subwavelength hole arrays of any size and with a broad range of possible patterns, depending on the master. In this study, we used inexpensive masters with cylindrical features spaced on the order of a micron. Work on fabricating films of hole arrays from more sophisticated masters, with features spaced less than 500 nm, is underway. This technology provides a flexible strategy to create large-area films of high optical quality, the properties of which can be tuned for sensing and device applications—especially those that combine SPPs for signal propagation with LSPs for coupling to and from the far-field. Furthermore, these films allow new applications of short wavelength plasmons (e.g., in aluminum) and versatile metal/dielectric composites for negative index applications at optical frequencies.

Acknowledgment. This work was supported primarily by the David and Lucile Packard Foundation and partially by an award from the Research Corporation and the URETI program of NASA (under Grant No. NCC 2-1363) subcontracted through Purdue University (under Agreement No. 521) at the MRI of Northwestern University. Theory work was supported by the National Science Foundation through the Northwestern Materials Research Center. The work at Argonne National Laboratory was supported by the U.S.

Department of Energy, Office of Basic Energy Sciences, Division of Chemical Sciences, Geosciences, and Biosciences under DOE Contract W-31-109-ENG-38.

References

(1) Ebbesen, T. W.; Lezec, H. J.; Ghaemi, H. F.; Thio, T.; Wolff, P. A. *Nature* **1998**, *391*, 667−669.
(2) Barnes, W. L.; Dereux, A.; Ebbesen, T. W. *Nature* **2003**, *424*, 824−830.
(3) Lezec, H. J.; Degiron, A.; Devaus, E.; Linke, R. A.; Martin-Moreno, L.; Garcia-Vidal, F. J.; Ebbesen, T. W. *Science* **2002**, *297*, 820−822.
(4) Devaux, E.; Ebbesen, T. W.; Weeber, J.-C.; Dereux, A. *Appl. Phys. Lett.* **2003**, *83*, 4936−4938.
(5) Chang, S.-H.; Gray, S. K.; Schatz, G. C. *Opt. Express* **2005**, *13*, 3150−3165.
(6) Williams, S. M.; Teeters-Kennedy, S.; Stafford, A. D.; Bishop, S. R.; Lincoln, U. K.; Coe, J. V. *J. Phys. Chem. B* **2004**, *108*, 11833−11837.
(7) Brolo, A. G.; Gordon, R.; Leathem, B.; Kavanah, K. L. *Langmuir* **2004**, *20*, 4813−4815.
(8) Brolo, A. G.; Arctander, E.; Gordan, R.; Leathem, V.; Kavanaugh, K. *Nano Lett.* **2005**, *4*, 2015−2018.
(9) Levene, M. J.; Korlach, J.; Turner, S. W.; Foquet, M.; Craighead, H. G.; Webb, W. W. *Science* **2003**, *299*, 682−686.
(10) Grupp, D. E.; Lezec, H. J.; Thio, T.; Ebbesen, T. W. *Adv. Mater.* **1999**, *11*, 860−862.
(11) Odom, T. W.; Love, J. C.; Wolfe, D. B.; Paul, K. E.; Whitesides, G. M. *Langmuir* **2002**, *18*, 5314−5320.
(12) Odom, T. W.; Love, J. C.; Thalladi, V. R.; Whitesides, G. M. *J. Am. Chem. Soc.* **2002**, *124*, 12112−12113.
(13) Henzie, J.; Kwak, E.-S.; Odom, T. W. *Nano Lett.* **2005**, *5*, 1199−1202.
(14) Hecht, B.; Bielefeldft, H.; Novotny, L.; Inouye, Y.; Pohl, D. W. *Phys. Rev. Lett.* **1996**, *77*, 1889−1892.
(15) Yin, L.; Vlasko-Vlasov, V. K.; Rydh, A.; Pearson, J.; Welp, U.; Chang, S.-H.; Gray, S. K.; Schatz, G. C.; Brown, D. B.; Kimball, C. W. *Appl. Phys. Lett.* **2004**, *85*, 467−469.
(16) Ordal, M. A.; Long, L. L.; Bell, R. J.; Bell, S. E.; Bell, R. R.; Alexander, R. W.; Ward, C. A. *Appl. Opt.* **1983**, *22*, 1099−1120.

NL051339S